AIAA SciTech Forum
8-12 January 2024, Orlando, FL
AIAA SCITECH 2024 Forum

10.2514/6.2024-0771

Large-scale multidisciplinary design optimization of a NASA air taxi concept using a comprehensive physics-based system model

Marius L. Ruh*, Andrew Fletcher†, Darshan Sarojini‡, Mark Sperry §,
University of California San Diego, 9500 Gilman Dr, La Jolla, CA 92093

Jiayao Yan¶, Luca Scotzniovsky ‖, Sebastiaan P. C. van Schie **, Michael Warner ††,
University of California San Diego, 9500 Gilman Dr, La Jolla, CA 92093

Nicholas C. Orndorff‡‡, Ru Xiang§§, Anugrah J. Joshy¶¶, Han Zhao***, Joshua J. Krokowski†††,
University of California San Diego, 9500 Gilman Dr, La Jolla, CA 92093

Hyunjune Gill‡‡‡, Seongkyu Lee§§§
University of California Davis, 1 Shields Avenue, Davis, CA 95616

Zeyu Cheng¶¶¶, Zhi Cao[17], Chris Mi[18]
San Diego State University, 5500 Campanile Dr, San Diego, 92182

Christopher Silva[19]
NASA Ames Research Center, Moffett Field, CA 94035

Lauren Wolfe[20]
Aurora Flight Sciences, A Boeing Company, 9950 Wakeman Drive, Manassas, VA 20110

J. S. Chen[21]
University of California San Diego, 9500 Gilman Dr, La Jolla, CA 92093

John T. Hwang[22]
University of California San Diego, 9500 Gilman Dr, La Jolla, CA 92093

Aircraft conceptual design is a high-dimensional optimization problem, involving up to hundreds of continuous design variables and constraints. The design of novel aircraft concepts such as electric vertical takeoff and landing (eVTOL) vehicles can benefit from the systematic

*PhD Student, Department of Mechanical and Aerospace Engineering, AIAA student member
†Ph.D. Student, Department of Mechanical and Aerospace Engineering, AIAA student member
‡Postdoctoral Scholar, Department of Mechanical and Aerospace Engineering, AIAA member
§Ph.D. Student, Department of Mechanical and Aerospace Engineering, AIAA student member
¶Ph.D. Candidate, Department of Mechanical and Aerospace Engineering, AIAA student member
‖Ph.D. Student, Department of Mechanical and Aerospace Engineering, AIAA student member
**Ph.D. Student, Department of Mechanical and Aerospace Engineering, AIAA student member
††Ph.D. Student, Department of Mechanical and Aerospace Engineering, AIAA student member
‡‡Ph.D. Student, Department of Mechanical and Aerospace Engineering, AIAA student member
§§Ph.D. Student, Department of Mechanical and Aerospace Engineering, AIAA student member
¶¶Ph.D. Candidate, Department of Mechanical and Aerospace Engineering, AIAA student member
***Ph.D. Student, Department of Mechanical and Aerospace Engineering, AIAA student member
†††Ph.D. Student, Department of Mechanical and Aerospace Engineering, AIAA student member
‡‡‡Ph.D. Student, Department of Mechanical and Aerospace Engineering, AIAA student member
§§§Professor, Department of Mechanical and Aerospace Engineering, AIAA associate fellow
¶¶¶Ph.D. Student, Department of Electrical & Computer Engineering
[17]Postdoctoral Researcher, Department of Electrical &; Computer Engineering
[18]Distinguished Professor and Chair, Department of Electrical & Computer Engineering
[19]Research Aerospace Engineer, Member AIAA
[20]Conceptual design engineer, Member AIAA
[21]William Prager Professor, Department of Structural Engineering
[22]Assistant Professor, Department of Mechanical and Aerospace Engineering, AIAA senior member

exploration of the design space through the use of gradient-based optimization. In this paper, we demonstrate the application of large-scale multidisciplinary design optimization (MDO) to NASA's lift-plus-cruise electric air taxi concept, using low and mid-fidelity physics-based simulations to model the aircraft. We improve the modeling fidelity from our previous work on the same air taxi concept through refined rotor-aerodynamic and aeroacoustic models as well as in-the-loop structural analysis. In addition, we expand the scope of the analysis to include several steady design conditions, a quasi-steady transition maneuver, structural sizing conditions, as well as one-engine-inoperative (OEI) scenarios, amounting to 18 design conditions. To perform the analysis and optimization, we use a newly developed software library called the Comprehensive Aircraft high-Dimensional Design Environment (CADDEE), which facilitates the integration of all discipline models. We solve a gross weight minimization problem with over 300 design variables and over 200 constraints, spanning all modeled disciplines. Results show a decrease in gross weight of 10% after a total optimization time of about 17 hours. These results demonstrate the effectiveness of applying of large-scale MDO to the aircraft conceptual design problem.

I. Introduction

There is a renewed interest in aircraft conceptual design due to a push toward electrified aviation in recent years driven, in part, by visions such as urban air mobility (UAM). Urban air mobility aims to provide on-demand and point-to-point delivery of passengers and payload in urban areas. Some of the key requirements to enable this technology are vertical takeoff and landing (VTOL) capabilities, electric or hybrid-electric propulsion architectures, high safety standards, and low noise emissions. In an effort address these requirements, over 700 [1] new VTOL concepts have been proposed, highlighting the importance of conceptual design to help select the most promising configurations.

Traditional conceptual design approaches [2–4] typically involve the use of regressions and semi-empirical models. Established software frameworks that employ this approach such as NASA's Flight Optimization System (FLOPS) [5], NASA's Design and Analysis of Rotorcraft (NDARC) [6], or the Common Parametric Aircraft Configuration Scheme (CPACS) [7] by the German Aerospace Center (DLR) provide fast evaluation times and reasonable accuracy for conventional aircraft and rotorcraft configurations due to an abundance of historically available data. This approach, however, is not viable for the evolving design space of UAM aircraft, which is not yet fully explored. Several software frameworks have been proposed in recent years to enable conceptual design of eVTOL and other novel aircraft concepts. NASA's successor to FLOPS, called the Layered and Extensible Aircraft Performance System (LEAPS) [8] was developed to enable conceptual design of new advanced concepts with a focus on (hybrid)-electric propulsion. Similarly, the Stanford University Aerospace Vehicle Environment (SUAVE) [9] was developed for unconventional aircraft configurations and augments regressions with low-fidelity physics-based models. Other noteworthy investigations and research that can improve the conceptual design of eVTOL aircraft is summarized as follows: a) sizing of hybrid-electric propulsion architectures [10–13] b) geometry-centric modeling and design [14, 15] c) trajectory optimization [16–19] d) preliminary sizing and weight estimation [20–22] e) fast vehicle conceptual design [23–26] and f) large-scale multidisciplinary design optimization [27–31].

A common feature of the previously mentioned research is the use of low-fidelity first-order approximations to model the aircraft. While this approach enables fast computation times, it limits model accuracy compared to physics-based models. In two recent studies [27, 28], we applied gradient-based large-scale MDO techniques in combination with physics-based models such as the vortex lattice method (VLM), blade element momentum (BEM) theory, tonal and broadband acoustic models, and others to optimize NASA's lift-plus-cruise UAM concept across multiple disciplines with over 100 design variables and 16 constraints. Some of the key limitations of these studies were the use of weight-regression models for structural sizing, low-fidelity aeroacoustic models, and limited mission analysis, which only included three steady design conditions.

In this paper, we build on the results from our previous investigations of the NASA lift-plus-cruise concept and expand the physics-based analyses to include 1) in-the-loop structural analysis, using beam models, 2) a quasi-steady transition maneuver, 3) one-engine inoperative (OEI) off-design conditions, and 4) improved aeroacoustic and rotor-aerodynamic models to account for edgewise flight conditions. We solve an optimization problem to minimize the gross weight of the lift-plus-cruise concept with respect to hundreds of design variables and constraints, using low to mid-fidelity physics-based models, with a total optimization time of less than one day. This is achieved by using a newly developed software library, called the Comprehensive Aircraft high-Dimensional DEsign Environment (CADDEE), whose critical features are automated adjoint-based sensitivity analysis, geometry-centric modeling, and modular data transfer. We demonstrate the feasibility of solving such a high-dimensional optimization within the allotted time to gain further insight into conceptual design considerations of UAM aircraft by refining our physics-based models and by including more advanced modes of operation in the analysis.

The remainder of this paper proceeds as follows. First, we give an overview of the aircraft design framework CADDEE in Sec. II. Then, we summarize the physics-based models used in this investigation in Sec. III. Next, we briefly cover our computational approach for solving the optimization problem in Sec. IV. Lastly, in Sec. V, we describe our test case, including the mission profile and optimization problem.

II. CADDEE design framework

CADDEE is a software library that enables the creation of multidisciplinary models of aircraft (and similar systems) to support analysis and design, using large-scale MDO. In this section, we summarize CADDEE's features such as its geometry-centric approach, its strategy for data transfer, and general framework architecture. We note that CADDEE is still under active development and not all of the described features are fully mature.

A. Design Parameterization

The design is parameterized using a high-fidelity representation of the outer mold line (OML). To achieve this, basis-spline surfaces are used due to their analytical form and their ability to effectively represent complex geometries with a small number of control points. These B-spline surfaces are then used to establish connections between any given set of external points and the central geometry using mapped arrays. A mapped array is a set of points resulting from the evaluation of a parametric map, which is determined by projecting points onto the OML. Mapped arrays serve various purposes, such as extracting meshes, determining geometric variables (e.g., wing area, rotation axes), and defining parameters for bulk actuation (e.g., tilting rotor or wing). By defining these mapped arrays based on the B-spline surfaces, any modifications made to the design geometry can be efficiently propagated through a simple matrix multiplication. This capability proves particularly valuable during optimization processes, where accurate representation of geometric variable changes, such as wing span or rotor location, is crucial for disciplines like aerodynamics and propulsion in order to capture the geometry changes. Figure 1a illustrates the application of mapped arrays, showing the generation of a camber surface mesh for the wing and horizontal tail superimposed with the B-spline geometry. In Fig. 1b, high-level sizing parameters like wing span and rotor radius are derived from relative distances using mapped arrays, visually depicted by the blue points.

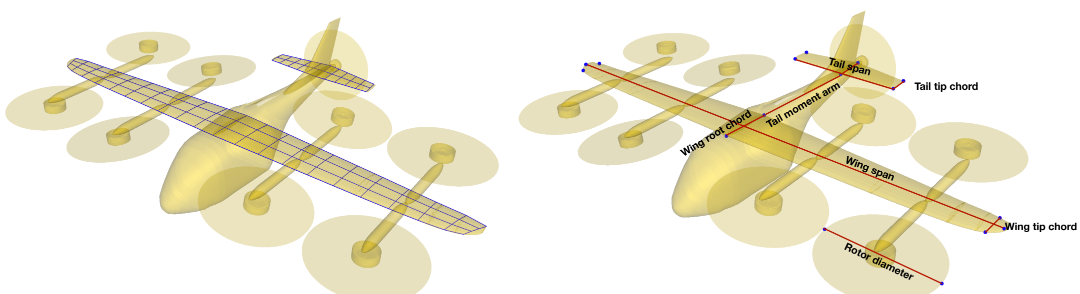

(a) Wing and horizontal tail camber mesh

(b) High-level geometric quantities.

Fig. 1 Illustration of the use of mapped arrays

B. Modular data transfer

The Solver-Independent Field Representation (SIFR) methodology [32] is a technique for unifying the representation of spatially-distributed quantities such as states, design variables, and other quantities of interest. This allows for a high level of modularity, as every solver interacts with a common, framework-level representation of all field quantities. Additionally, SIFR enables modular, invariant-conservative coupling by coupling each solver to the framework representation, rather than directly together.

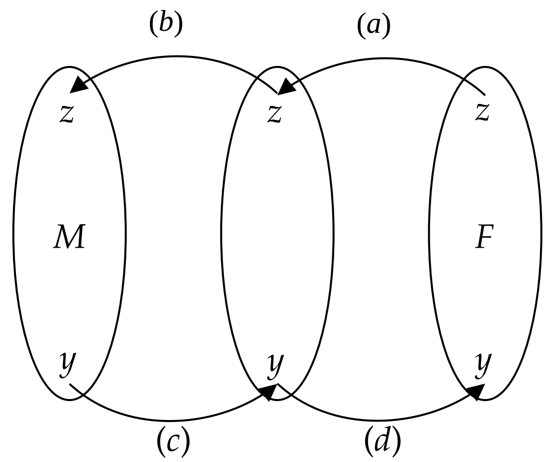

Fig. 2 Illustration of the SIFR process between framework (F) and model (M) with input z and output y: (a) framework evaluation, (b) model input, (c) model output, (d) framework fitting

This is achieved by treating field quantities in a similar manner to the geometry. Each sub-surface in the geometry acts as a map from its parametric space to physical space. This geometry information is then passed to solvers via a mesh of points in space. Similarly, each field quantity is represented by a union of maps from the aforementioned parametric spaces to its state-space. Then, this field information can be passed to solvers via a similar mesh of points in space. Each field can be updated by fitting its map to incoming data. This process is shown in Fig. 2.

C. Comprehensive analysis

CADDEE has the capability to simulate various aircraft design disciplines across multiple mission segments, accommodating different levels of fidelity within discipline models. Models of the same type are efficiently applied across mission segments by leveraging vectorization techniques. The mission segments can be categorized into three types. Firstly, trim-state segments represent steady operational conditions, such as cruise or hover, and are relatively straightforward to analyze. Secondly, transient segments involve time integration schemes to capture dynamic transitions or gust responses, making them computationally more demanding. Lastly, the third type of mission segment focuses on off-design conditions, such as flutter or aeroelastic divergence.

D. Automated adjoint-based sensitivity analysis

One of the key features of CADDEE is that of automated sensitivity analysis, which is enabled by implementing the CADDEE framework in the newly developed computational system design language (CSDL) [33]. This is an embedded domain specific language, designed for easily solving multidisciplinary analysis and optimization (MDAO) problems, while automating the computation of derivatives across individual and coupled disciplines. CSDL operates at a high-level of abstraction, allowing the engineer to construct mathematical models using familiar Python syntax. By implementing CADDEE using CSDL, the engineer can systematically search a potentially high-dimensional design space, using gradient-based optimization to find the optimal aircraft design

E. Framework architecture

In Fig. 3 we show the general architecture of the CADDEE framework in the form of a design structure matrix (XDSM) for a gneral example of an aircraft design problem for which CADDEE could be used. The diagram shows how disciplines are connected, what constraints are enforced (indicated by c) and what variables are optimized (i.e., design variables). In this example, the cost analysis outputs the objective function (indicated by f). In general, this can be any other quantity of interest such as gross weight, range, noise etc. The geometry model takes in geometric design variables (e.g., wing span, wing area) and motion design variables (e.g., tilt rotation) and outputs an actuated geometry that contains meshes and other geometric quantities needed by different disciplines. Next, the actuated geometry, along with information about the material and thicknesses, is passed into the mass properties model, which computes aircraft-level mass properties from individual subsystem components.

The next block on the main diagonal, loosely labeled “Aeromechanics”, contains the bulk of the analysis, vectorized across all mission segments, indicated by the stacked shapes. Models that are included in the aeromechanics block are aerodynamics, propulsion, structural analysis, stability and control, as well as acoustics. In general, coupling between disciplines may arise such as aero-structural or aero-acoustic coupling. Typically, inputs to the aeromechanics block are the previously computed mass properties, actuated geometries, and the operating conditions of the aircraft (e.g., speed, flight path angle, rotor rotational speed etc.). Some outputs of the aeromechanics block can also be constraints such as the trim state of the aircraft (equations of motion residuals), stability and control (handling qualities), or acoustics (noise maps). Other aeromechanics outputs are passed into the last major analysis block, which models the powertrain and energy consumption. Depending on the powertrain architecture (e.g., eVTOL vs. hybrid-electric), inputs are the torque required by the rotors and the total time spent in each mission segment. These are required inputs to the motor analysis model to compute a power profile for the mission. The power profile is then used by the battery model to estimate the final state-of-charge, which may be a constraint during optimization. We note that intermediate components such as inverters and gearboxes that connect motors, batteries and rotors, may also be modeled. Lastly, the output of the powertrain and energy analysis is the total energy used, which can be passed into the cost analysis along with the aircraft gross weight to compute quantities such a direct operating cost, if such a model is implemented.

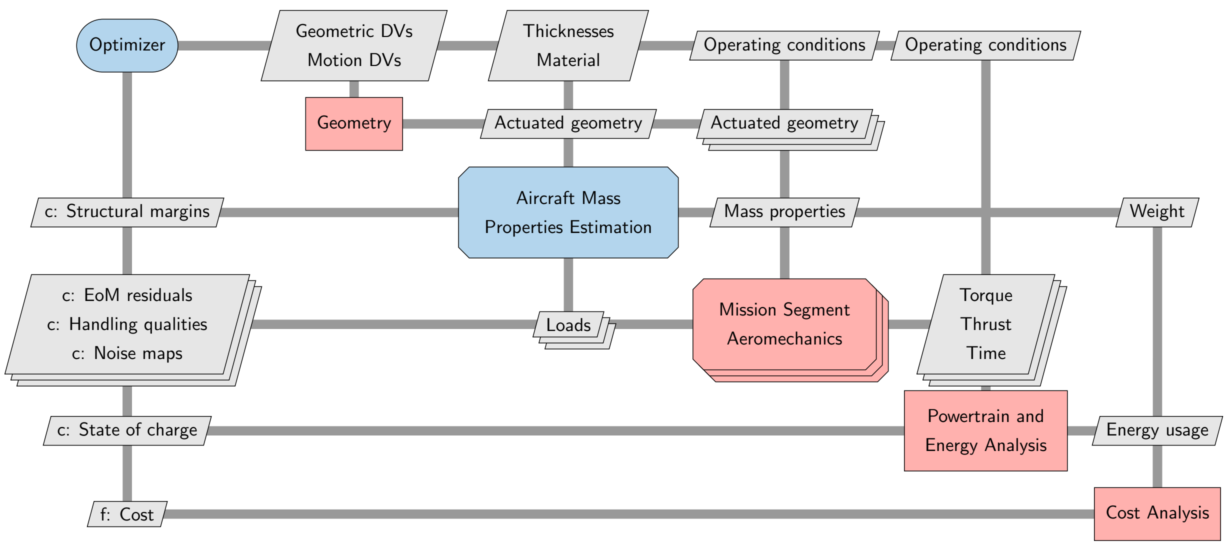

Fig. 3 Architecture of the CADDEE design framework

III. Physics-based models

A. Aerodynamics

1. Wing aerodynamics

We developed a fluid solver called Vortex-based Aerodynamic Solver Toolkit (VAST) for the aerodynamic analysis. It has multiple solver options: lifting-line method (LLT), vortex lattice method (VLM), and vortex panel method. VAST has options for both static and dynamic simulations. Vortex-based methods are a set of commonly used methods to analyze the aerodynamic performance, such as force or pressure distribution of lifting surfaces [34]. Vortex-based methods assume the flow to be a potential, characterized by an irrotational velocity field, which is given by

$$\nabla^2 \Phi = 0 \,, \tag{1}$$

where Φ is the fluid potential.

Other assumptions for the solver include that 1) the fluid is incompressible and inviscid; and 2) the lifting surfaces are thin with a small angle of attack and sideslip. In addition, VLM assumes the lifting-surface to be thin, while panel methods consider the thickness of the airfoil. Figure. 4 demonstrates the inputs, model, and outputs of VAST. The

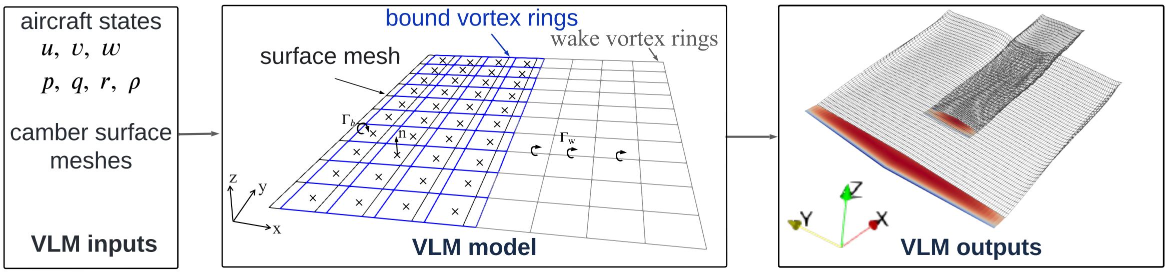

Fig. 4 Aerodynamic analysis solution process

inputs of VAST are the meshes and the states of the lifting surfaces. VAST uses structured quadrilateral panels. The outputs of the VAST model are the pressure on each panel given by panel forces divided by the area. The panel forces are calculated using the Kutta–Joukowski theorem [35] for the VLM option and we use Bernoulli's principle to compute the traction forces for the panel method.

2. Rotor aerodynamics

In this study, we use blade element momentum (BEM) theory whenever appropriate, meaning in mission segments where the rotor disks are largely perpendicular to the freestream velocity (e.g., hover, climb, cruise). Under these operating conditions, BEM methods provide reasonable accuracy and fast evaluation times. The theory has been well-established for rotors, propellers, as well as wind turbine analysis and is described in many papers and textbooks (see e.g., [36–41]). BEM theory combines blade element and momentum theory. In the former approach, the blade is discretized into individual elements (i.e., airfoils), which are modeled independently of each other. The latter approach models the rotor as an actuator disk and only considers the change in momentum of the air due to the action of the rotor. By combining blade element and momentum theory, we obtain two equations for sectional thrust and sectional torque, each, which are combined to form a residual equation in terms of the sectional inflow angle. Solving this residual equation robustly is crucial and implementations with provable convergence exist (see e.g., [42, 43]).

It is important to note that momentum theory is based on a streamtube (control volume) analysis, which is most accurate for axial flow conditions. For conditions, in which the blades are exposed to edgewise flow (i.e., the rotor disk is parallel to the flow), such as transition from and to hover, BEM theory does not provide reasonable accuracy. For such cases, we make use of a dynamic inflow model by Pitt and Peters [44, 45]. This model provides reasonable accuracy for edgewise flight conditions.

B. Structural analysis

Structural weight estimation techniques for conventional aircraft often rely upon statistical methods or simple, energy-based formulas. Unconventional aircraft, including many air taxi concepts, cannot use these methods because the configuration of the aircraft is unique, and is not well represented by any existing data. This challenge motivates the use of physics-based structural weight estimation for sizing air taxis.

Within the context of a larger multidisciplinary optimization problem, structural weight estimation is only one of several solvers. Therefore, the goal is to develop a structural solver with just enough fidelity to capture changes in aircraft weight with regards to the design variables without a large computational expense. To this end, we choose to implement a linear Euler-Bernoulli beam model [46]. This model represents slender aircraft structures (wing, fuselage, booms etc.) as one-dimensional beams. The entire structural system is represented by a global stiffness matrix K. When considering a nodal-loads vector F, the nodal displacements U are found by solving a single linear system:

$$F = KU. \tag{2}$$

The stiffness matrix is constructed using 12×12 frame stiffness elements [47]. These elemental stiffness matrices use simple tube and box-beam representations when computing cross-sectional properties. For example, a wing can be reasonably represented by a box-beam and a fuselage by a tube [48] [49]. By optimizing the thicknesses of the cross-section in question, we can find the minimum-mass structure given certain constraints. The most basic constraint is the maximum allowable stress or displacement. However, many slender structures like wings will instead be sized by buckling constraints. To capture this we calculate the critical panel-buckling stress as a function of skin thickness t, panel width b, and the constant k which is a tabulated function of the panel's aspect ratio [50]:

$$\sigma' = k\frac{E}{1-\nu^2}\left(\frac{t}{b}\right)^2. \tag{3}$$

For stress-constrained structures we perform a stress-recovery based on the nodal displacements and a selection of stress-evaluation points on the cross section. For box beams, the Von-Mises stress is evaluated at five points that are expected to reasonably capture the maximum axial, bending, and shear stresses under typical loading conditions [48].

For this study, the material of choice is aluminum alloy. Due to the limitations of the box-beam model, which assumes constant cross-sectional properties (i.e., we cannot model stiffeners), we expect to over-predict the mass of the wing box and do not apply a safety factor for buckling constraints. To capture variations in the cross-sectional properties, higher-order beam models such as the variational asymptotic method (e.g., [51]) are necessary.

Lastly, we note that the beam model is used only to size the wing box. For other structural components such as the tail or the fuselage, we use weight regression models developed specifically for the lift-plus-cruise concept [22], which we used in our previous studies.

C. Stability

For this work, we assume small disturbances only, for which the system dynamics can be written as

$$\dot{\vec{x}} = A\vec{x} + B\vec{u} \tag{4}$$

where $\dot{\vec{x}}$ is the time derivative of the state vector, which includes linear and angular accelerations of the aircraft with respect to its body-fixed reference frame. Lastly, A and B are the state and control derivative matrices, respectively.

To determine stability, eigen-analysis is applied to the A matrix, which is constructed about the trim (i.e., steady) conditions for the mission segments that we consider. For example, consider two steady mission segments: hover and cruise. In this case, the 12×12 A matrix is constructed about the trim condition for each segment and the matrix is divided into longitudinal and lateral matrices, each of size 4×4. We construct the stability matrices using a backward finite difference approximation of the derivative of the aircraft accelerations with the respect to the aircraft states. Next, the eigen-modes are computed to obtain the frequency response and damping ratios. These parameters are determined with respect to handling qualities constraints (see e.g., [52, 53]). For cruise segment constraints, we follow the MIL-F-8785C Flying Qualities of Piloted Airplanes [54] and for hover segment constraints, we follow ADS-33E-PRF Handling Qualities for Military Rotorcraft [55].

D. Aeroacoustics

Low-fidelity aeroacoustic prediction tools offer the advantage of efficient computation time with reasonable accuracy; this is key during the preliminary aircraft design phase. This has been demonstrated by Sarojini et al. [56] and Orndorff et al. [57], who have applied low-fidelity aeroacoustic tools to optimization problems for electric vertical-take-off-and-landing (eVTOL) aircraft. The aeroacoustic models utilized in these studies, specifically the Barry–Magliozzi [58] and Schlegel–King–Mull [59] models, provided valuable insight into how tonal and broadband noise are influenced by changes in aircraft design. However, these models are limited to steady hover and axial flight conditions. Higher fidelity tools are required to capture the unsteadiness in other flight orientations, such as edgewise forward flight. In this work, the Lowson and Ollerhead's (LO) model [60] is employed to predict tonal noise, and the Gill and Lee's (GL) machine-learning-based broadband noise spectrum model [61] is used to predict broadband noise. The LO model accounts for the fluctuation of forces along the azimuth, thus being applicable in an edgewise forward flight condition. The GL model accounts for azimuthal variation through the thrust coefficient and retreating blade speed; validation studies have shown reasonable accuracy in edgewise flight. Furthermore, the GL spectrum model provides a more comprehensive broadband noise analysis in hover by predicting the noise spectrum across a range of frequencies. These two models are capable of predicting noise profiles at all flight conditions.

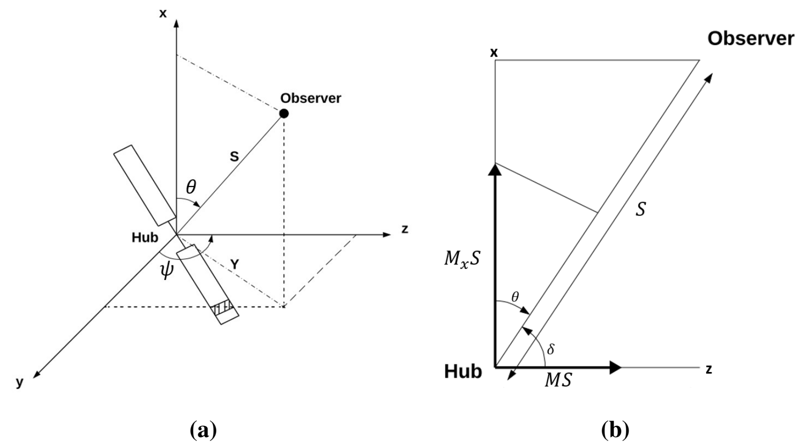

Fig. 5 (a) Coordinate system used in the tonal noise prediction models and (b) integration of forward motion into the LO model.

Tonal Noise: Lowson-Ollerhead

Lowson and Ollerhead [60] (LO) developed a loading noise model utilizing the variation of aerodynamic loads along the azimuth to account for unsteady loading. The thickness noise component is ignored in the LO model, as the unsteady loading is the dominant noise source. However, the model by Barry and Magliozzi [56–58, 62] can be used in hover or axial forward flight to account for thickness noise. The variation of the loads along the azimuth is expressed using the cosine-sine form of Fourier series. The azimuthally varying thrust and drag at a single radial location is defined as:

$$\begin{aligned} T(\psi) &= a_{0T} + \sum_{\lambda=1}^{\infty} a_{\lambda T}\cos(\lambda\psi) + b_{\lambda T}\sin(\lambda\psi) \\ D(\psi) &= a_{0D} + \sum_{\lambda=1}^{\infty} a_{\lambda D}\cos(\lambda\psi) + b_{\lambda D}\sin(\lambda\psi). \end{aligned} \tag{5}$$

Using the Fourier coefficients of the unsteady loads, the final formulation of the model is derived as follows:

$$\begin{aligned} c_{mB} = \frac{mB^2\Omega}{4\pi c S}\int_{hub}^{tip}\sum_{\lambda=0}^{\infty} i^{-(mB-\lambda)}\Bigg\{\frac{x}{S}\Big[i a_{\lambda T}(J_{mB-\lambda} + (-1)^{\lambda}J_{mB+\lambda}) - b_{\lambda T}(J_{mB-\lambda} - (-1)^{\lambda}J_{mB+\lambda})\Big] \\ - \Bigg[\frac{i a_{\lambda D} c}{mBR\Omega}\big((mB-\lambda)J_{mB-\lambda} + (-1)^{\lambda}(mB+\lambda)J_{mB+\lambda}\big) - \frac{b_{\lambda D} c}{mBR\Omega}\big((mB-\lambda)J_{mB-\lambda} - (-1)^{\lambda}(mB+\lambda)J_{mB+\lambda}\big)\Bigg]\Bigg\} dR \end{aligned} \tag{6}$$

where J_ν is the Bessel function of the first kind with the following arguments:

$$J_\nu = J_\nu\left(\frac{mB\Omega R}{c}\sin\theta\right). \tag{7}$$

The coordinate system for the tonal noise predictions by the LO model is provided in Fig. 5a. For the purpose of the current study, the radial force component is assumed to be negligible. With this assumption, Lowson's unsteady loading noise model collapses into the Gutin's steady loading noise model [63] when $\lambda = 0$; as a result, the loading noise along the rotor axis cannot be accurately predicted. To resolve this issue, the Sears function [64] presented by Kvurt and Stalnov [65] is employed to represent the unsteady loading using the steady loads from blade element and momentum (BEM) theory. To account for motion of the rotor hub, a Doppler correction is applied to the hub-observer distance S using the Mach number in the direction of the observer M_r. The adjusted hub-observer distance becomes $S(1 - M_r)$, represented visually in Fig. 5b. The final sound pressure level (SPL) of the tonal noise in decibel (dB) is expressed as:

$$\mathrm{SPL_{Rotor}} = 10\log_{10}\left(\frac{|c_{mB}|^2}{2P_{ref}^2}\right) \tag{8}$$

where $P_{ref} = 2 \times 10^{-5}$.

Broadband: GL Spectrum

The GL spectrum model [61] is used to predict the broadband noise spectrum and the overall sound pressure level (OASPL). The GL spectrum model is a data-driven empirical broadband noise spectrum model developed using an evolutionary machine learning algorithm called Gene Expression Programming (GEP); experimental data from modern rotors, such as drone rotors [66, 67] and urban air mobility (UAM) proprotors [68], was utilized in the GEP algorithm. The development process and the detailed description of the machine learning algorithm can be found in the references [61, 69, 70]. The pre-determined functional form of this model is given as

$$\mathrm{SPL}_{1/3} = \frac{f_0 \Delta^{0.6}}{[f_3 \Delta^{f_4} + f_5]^{f_6} + [f_7 \Delta]^{f_8}} \tag{9}$$

where $\Delta = S_t - (f_1 \log_{10} C_T + f_2 \log_{10} \sigma)$, $S_t = \frac{fc}{V_t}$ is Strouhal number based on the solidity-weighted chord length ($c = \frac{\sigma \pi R}{N}$), C_T is thrust coefficient, σ is rotor solidity, $f_0 = 10 \log_{10} V_t^{7.84}$. The functions f_1 through f_8 are obtained by the GEP algorithm. The basic form of the GEP spectrum model shown in Eq. (9) is based on a universal wall pressure spectrum model [71] since this wall pressure spectrum determines a primary shape of trailing-edge noise [72], which is a major rotor broadband noise source [73]. The function f_0 controls the amplitude of the spectrum; based on a maximum SPL analysis, the noise level scales best with the blade tip velocity to the power of 7.84. The complete set of functions are given as:

$$\begin{aligned}
f_0 &= 10 \log_{10} V_t^{7.84} \\
f_1 &= \sigma \\
f_2 &= 0.9 M_t \sigma (M_t + 3.82) \\
f_3 &= 1 \\
f_4 &= 1 \\
f_5 &= -2 M_t^2 + 2.06 \\
f_6 &= -C_T M_t (C_T - \sin|\theta_0| + 2.06) + 1 \\
f_7 &= C_T \\
f_8 &= 4.97 C_T \sin|\theta_0| (1.5(S/R)) M_t - (S/R) + 15)
\end{aligned} \tag{10}$$

where M_t is blade tip Mach number, θ_0 is the elevation angle measured from the rotor plane, S is the observer distance from the rotor hub, and R is rotor radius. Although this model is derived from a series of experiments on various hovering rotors, some preliminary validations demonstrated sufficient predictive performance even in an axial and edgewise forward flight conditions [74]. The model does not directly account for the forward motion; however, the variations in the thrust coefficient due to the axial motion of a rotor indirectly affect the prediction of the broadband noise in the axial forward flight conditions. Additionally, validations studies conducted using helicopter rotor data showed that the GL spectrum model can reasonably predict noise levels in the edgewise forward flight condition when the minimum tip velocity at the retreating side of the rotor was used as an input; further validation studies in different rotors and operating conditions are required.

E. Motor Analysis

The propulsion and motor discipline in electric aircraft system level analysis plays an important role in weight estimation and overall estimation of electric power consumption. A study conducted by Vegh et. al. [75] focused on the existing challenges of electric vertical take-off and landing (eVTOL) aircraft by estimating the weight and performance of a single reference mission; it was found that the electric propulsion system accounted for roughly 40 % of the gross takeoff weight. In a system-level setting, the motor discipline is commonly represented using generalized data-driven relationships, neglecting the internal topology and physics of the motor; this includes constant efficiency assumptions [76] and simple weight estimation models based on empirical torque-to-weight [75] and power-to-weight ratios [77]. These approaches are practical for preliminary sizing estimates but are limited in scope and reach. The motor model developed for this project aims to analytically represent the motor sizing and performance with a physics-based approach, and increase the fidelity of preliminary models. This low-fidelity model is divided into two main sub-models: sizing and performance; a detailed architecture is displayed in Figure 6.

The motor sizing calculates the motor geometry based on simplified empirical relationships found in [78]. These relationships determine two main subsets of the motor geometry: large-scale geometric parameters such as rotor radius

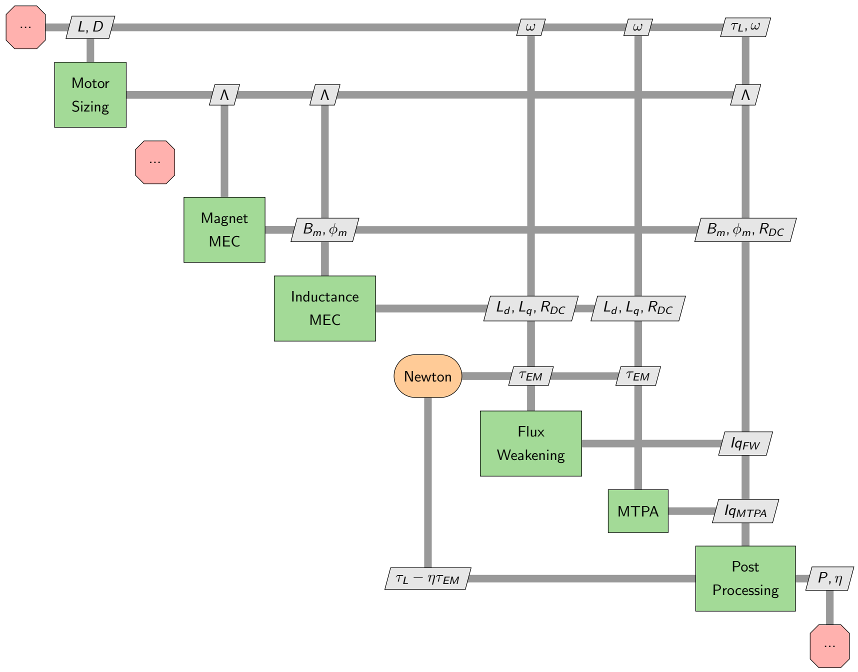

Fig. 6 Motor Model Architecture

and motor mass, and internal motor sizing parameters like air-gap depth and stator tooth width. Both subsets of the geometry are incorporated in different areas of the motor performance analysis. The comprehensive set of geometric variables in Figure 6 are represented with Λ.

The performance model determines the efficiency and power output for each load case, which utilizes the motor geometry from the sizing model and the speed and load torque for each operating case. The performance model determines the operating electromagnetic torque implicitly using a Newton solver. The residual is

$$R = \tau_{load} - \eta\tau_{EM} = 0, \tag{11}$$

where τ_{EM} is the electromagnetic torque and η is the motor efficiency determined by the outputs of the flux weakening and MTPA (maximum torque per ampere) control methods. A magnetic equivalent circuit formulation is implemented based on [79] to estimate internal magnetic and electric components such as magnet strength and inductance. These outputs are then incorporated to determine the current based on operating voltage using a smoothed formulation of two discrete control modes: flux-weakening [80] and MTPA [81]. The flux-weakening control method operates at the voltage limit, while MTPA governs the operation below the voltage limit. The output power and efficiency are then computed based on the resultant operating current. For this study, we do not consider flux-weakening since the rotor torque requirement is unlikely to exceed the critical threshold for flux-weakening to set in.

F. Battery Sizing and Analysis

In this study, we employ a simplified approach to battery sizing and analysis. The optimizer controls the battery mass, designated as m_{bat}. Given a battery mass m_{bat} and a battery energy density ρ_{bat} (Wh/kg), the total energy capacity of the battery (E_{total}) is calculated as

$$E_{\text{total}} = (\rho_{\text{bat}} \cdot 3600)\left(\frac{m_{\text{bat}}}{1000}\right) \tag{12}$$

We assume a future battery technology with a pack-level energy density of 400 Wh/kg. Denoting the power profile as $P(t)$, time as t, and the total mission time as T, the end-of-mission state-of-charge is determined by

$$SoC = E_{\text{total}} - \frac{\int_0^T P(t)dt}{E_{\text{total}}}. \tag{13}$$

The power is obtained for each on-design design condition (i.e., mission segment) and multiplied by the time spent in each mission to compute the corresponding energy expenditure.

IV. Computational approach

A. Parallelization

In order to achieve our objective of solving the optimization problem within the prescribed amount of time (<10 hrs), utilization of parallelization is required. Our approach [82] uses a static scheduling algorithm that integrates automatic message-passing operations in the evaluation function of the numerical model using OpenMPI [83]. The scheduling method is a heuristic algorithm based on list scheduling, which is designed to minimize maximum final processor time. Prior to execution, it analyzes the computational graph of the optimization model and determines the optimal partitioning of tasks to a given number of processors [84].

B. Optimization

Our target optimization problem is inherently large-scale, characterized by hundreds of design variables and tens of constraints. Sequential quadratic programming (SQP) and interior point (IP) methods have proven highly effective for solving large-scale optimization problems, typically requiring hundreds or fewer model evaluations. For our problem, we plan to use the SNOPT [85] optimization algorithm which is based on the SQP method. Since our system model contains multiple subdiscipline models, the magnitudes of design variables could span different orders of magnitude. The resulting poor scaling and the lack of good initial guesses for some of the design variables could lead to convergence issues during the optimization. To mitigate these issues, we will perform subsystem level optimizations and utilize the resulting solutions to appropriately scale and initialize the overarching system-level optimization problem.

V. Test case: The NASA lift-plus-cruise concept

As stated before, the UAM concept vehicle that we consider in this study is NASA's lift-plus-cruise concept. This is a fixed-wing concept with eight lift rotors mounted on the main wing. These rotors are only activate during vertical ascent and descent, as well as during transition maneuvers. As such, these rotors are not intended to provide significant thrust and will only produce small aerodynamic forces and moments during cruise, in which a so-called pusher-propeller that is mounted at the rear provides the necessary thrust.

In Fig. 7, we show the mission profile that we consider in this study, which is adopted from a study by Silva et al. [86]. The red color indicates the mission segments that we model. The mission includes a a hover segment, a quasi-steady outbound transition segment, a climb segment, a cruise segment, a descent segment, and another hover segment. For the quasi-steady transition, we assume a constant altitude and use the results from studies by Orndorff et al. [17, 18], in which a minimum-energy transition trajectory for the lift-plus-cruise vehicle was determined by integrating the equations of motion. We discretize the optimal trajectory with ten points, for which we constrain the lateral acceleration. The total mission profile is repeated a second time and a cruise reserve is added. At the end of the mission, we require a final battery state-of-charge of at least 20%. A detailed breakdown of what physics-based models are used in each segment is shown in Tab. 1.

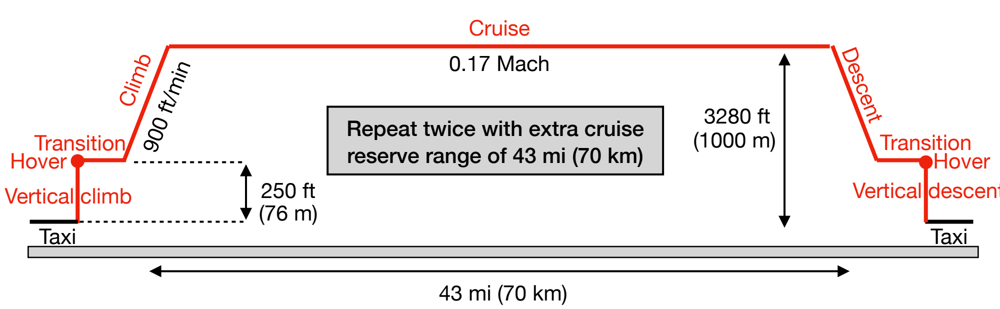

Fig. 7 Mission profile for this investigation

Table 1 Summary of design conditions and physics-based models used

discipline/ design condition	*rotor aero*	*wing aero*	wing structure	*aeroacoustics*	*motor*
+3g sizing	BEM	VLM	EB beam	–	–
-1g sizing	BEM	VLM	EB beam	–	–
OEI (x4)	BEM	–	–	–	ECM
hover	BEM	–	–	tonal: Lowson broadband: GL	ECM
quasi-steady transition (x10)	Pitt–Peters	VLM	–	tonal: Lowson broadband: GL	ECM
climb, cruise, descent	BEM	VLM	–	–	ECM

VI. Results

In this section, we present two sets of results. In Sec. VI.A, we focus on the improved modeling fidelity over our previous studies of the lift-plus-cruise concept [27, 28]. We show the results of a structural sizing optimization, as well as a noise directivity plot of the aircraft in various flight conditions. In Sec. VI.B, we present the result of our full-scale optimization study, in which the optimizer can change all (including geometric) variables of the design.

A. Sub-scale MDAO

Due to the complexity of this high-dimensional optimization problem, we warm-start the system-level optimization via two sub-scale optimizations. In these optimizations, we do not change the aircraft geometry and simply aim to obtain a good starting point for the large-scale optimization.

First, we size the wing structure through two sizing conditions (see Tab. 2a), in which the aircraft is subjected to plus 3g and minus 1g loads, respectively. These load-cases will size the top-and bottom skin thicknesses as well as the spar thickness. We aim to minimize the wing weight subject to buckling, stress, and displacements constraints. Second, we perform an aircraft trim optimization, such that the forces and moments during each steady design condition are close to zero. Here, the optimizer is only given the freedom to optimize trim variables such as the rotor speeds, aircraft pitch angle, and the elevator deflection. For quasi-steady transition points, we constrain the accelerations, according to our discretized transition profile (see Sec. V).

1. Wing-box sizing

In Fig. 8, we show the thicknesses of the top and the bottom skin of the box beam after applying the plus 3g and minus 1g load cases. As expected, the load cases size the top and bottom skin thicknesses differently, with the plus 3g load case sizing the top skin, and the minus 1g load sizing the bottom skin, which is thinner than the top. We find (not shown) that the buckling constraint is indeed the sizing criterion and that the strength and displacement constraints are inactive. For the initial wing geometry (i.e., before the full-scale optimization), the wing-box mass is about 370 kg. Lastly, in Fig. 9, we show the (magnified) deflection of the wing for both load cases, compared to the undeformed geometry.

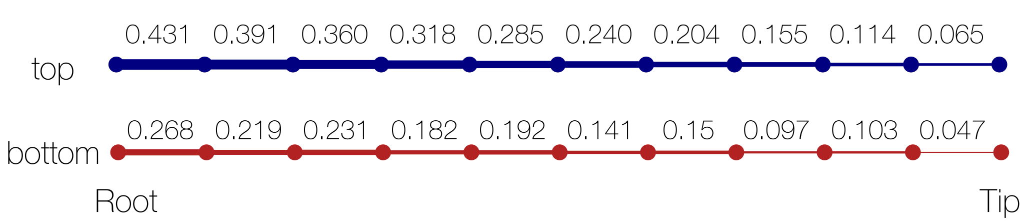

Fig. 8 Top and bottom skin thickness (in) of the initially sized box beam

(a) Wing sizing

	Variable/function	Quantity
minimize	wing structural mass	
w.r.t.	spar thickness	21
	top skin thickness	21
	bottom skin thickness	21
	trim residual norm	2
	aircraft pitch angle	2
	elevator deflection angle	2
	propeller speed	2
	# design variables	71
subject to	buckling constraints (2x20)	40
	maximum stress (5x20)	100
	maximum displacement (3x21)	63
	beam symmetry (3x10)	30
	aircraft accelerations	2
	# constraints	235

(b) Trim

	Variable/function	Quantity
minimize	aircraft acceleration	
w.r.t.	lift rotor speeds (8x14)	112
	propeller speeds (1x16)	16
	aircraft pitch angle	16
	elevator deflection	15
	# design variables	149

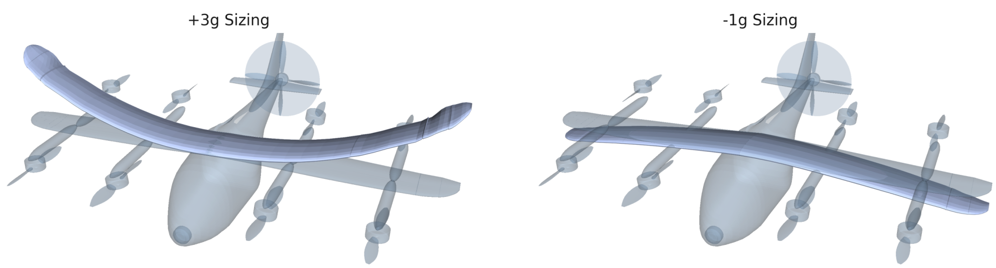

Fig. 9 Wing deflection for +3g and -1g load cases (x20 magnification)

2. Aeroacoustic analysis of the lift-plus-cruise vehicle

Noise profiles are visualized to assess aircraft acoustic levels in space and time. These profiles from different mission segments near the ground are compared to understand how noise changes during the initial flight segments, where there is concern of disturbing the surrounding space of the aircraft at low altitudes. In Fig. 10, we show a noise (A-weighted decibel) directivity plot of the vehicle for different flight conditions: hover and five out of ten quasi-steady transition points. At each transition point, the aircraft hovers or transitions at an altitude of 250 ft above the ground and the sound-pressure level is observed along a semi-sphere, starting from the aircraft plane. We see that the aircraft emits ths most noise during the first transition point, at which the aircraft experiences the highest acceleration at just over $3m/s^2$, provided by the propeller. At the same time, the aircraft's speed is low, which means that most of the lift is provided by the lift rotors. This combination of lift rotors and the propeller is a likely explanation for the high noise footprint during the first transition point. At the later transition points, the aircraft's acceleration decreases while the speed increases, which means that more lift is provided by the wing and the rotors' noise contribution decreases. An interesting observation of the directivity plot is the asymmetry, which is more pronounced for the later transition point (e.g., transition 9) and is a likely manifestation of the Doppler effect with increasing aircraft speed.

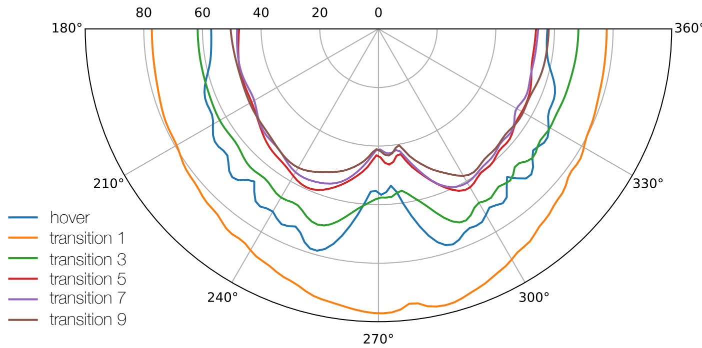

Fig. 10 Directivity plot of the lift-plus-cruise vehicle

3. Longitudinal aircraft stability

In Fig. 11, we show the eigenvalues of the short-period and Phugoid stability modes for lift-plus-cruise vehicle in cruise. We see that the aircraft is stable in both modes, with the Phugoid mode being less stable. Based on these eigenvalues, the natural frequency, damping ratio, and time to double for the short-period mode are computed as 3.61 Hz, 0.22, and 0.86 s, respectively. For the Phugoid mode, the same quantities are 0.25 Hz, 0.28, and 9.83 s. While for this optimization we do not constrain these quantities according MIL-F-8785C Flying Qualities of Piloted Airplanes [54], we plan to do so in future studies.

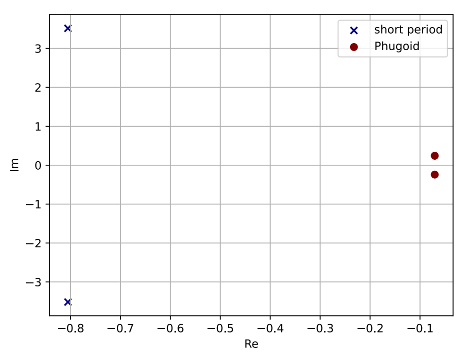

Fig. 11 Eigenvalues for longitudinal stability

B. Full-scale MDO

In this section, we present the results of the full-scale optimization (gross weight minimization) problem we solve, shown in Tab. 3. At a high level, the design variables can be categorized into geometric (e.g., wing area, rotor radii), operational (e.g., aircraft pitch, rotor speed), and sizing variables (e.g., skin thickness). We note that not all design variables listed may be of relevance for practical applications. An example is the (lift) rotor disk disk angle (±5°), which we optimize for all design conditions in which the lift rotors are active. Although the lift-plus-cruise concept proposes fixed lift rotors to reduce design complexity, we include the rotor disk tilt design variables for two reasons: 1) to facilitate aircraft trim and 2) to demonstrate the feasibility of including a large number of rotor actuation parameters for potential future work on other eVTOL aircraft such as tilt-rotor concepts. The constraints we impose can be loosely grouped into operational (aircraft trim), safety (stress and displacement)*, acoustics, and geometry symmetry constraints.

A detailed breakdown of the aircraft component weights before and after the optimization is shown in Fig. 12. The optimized gross weight is about 7100 lb (3220 kg), which is a decrease of about 10% or 650 lb compared to the initial design. About 45% of this decrease can be attributed a smaller battery, whose weight is 300 lb lighter.

*We note that for the full-scale optimization, buckling constraints are not imposed, which will be corrected in future studies

Table 3 Full-scale MDO problem

	Variable/function	Quantity	Variable/function	Quantity
minimize	wing vehicle gross mass			
w.r.t.	rotor radii	8	blade twist (4x9)	36
	blade chord (4x9)	36	motor length	9
	motor diameter	9	wing AR	1
	wing area	1	wing twist	10
	horizontal tail AR	1	horizontal tail area	1
	tail moment arm	1	battery mass	1
	disk tilt angle	124	horizontal tail deflection	14
	lift rotor speed	62	propeller speed	10
	vehicle pitch angle	12	top skin thickness	20
	spar thickness	20		
	# design variables	376		
subject to	trim residual norm	18	Sound pr. level	5
	final state of charge	1	beam stress/displacements	163
	max. motor torque	5	geometry symmetry	46
	# constraints	238		

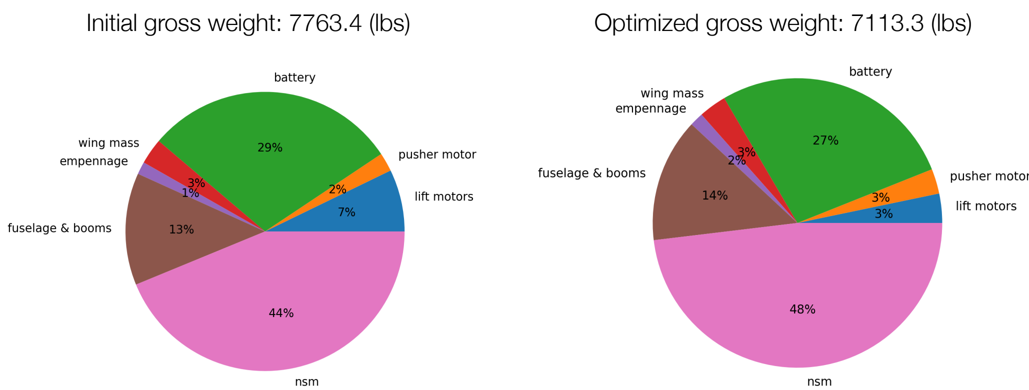

Fig. 12 Weight breakdown before and after optimization

1. Design feasibility

To demonstrate the optimized design's feasibility, we show multiple optimization constraints as a function of the optimization iteration in Fig. 13. One of the key constraints is that the aircraft has to be trimmed for every steady design condition. To this end, we show the aircraft trim residual as a function of the optimization iteration for all steady design conditions. We observe a decrease of several orders of magnitude for all design conditions as the optimization progresses. Since the trim residual is a representation of the aircraft's linear and angular accelerations, we conclude that for steady design conditions, the optimized aircraft experiences net forces and moments on the order of a few Newton (meter), which demonstrates that the aircraft is trimmed. Next, we note that the noise constraint, which is set at 75 dB-A at an observer distance of 250 feet below the aircraft, is also met. Lastly, we show the optimized power profile against the mission time and see that the final state-of-charge constraint of 20% at mission end is satisfied.

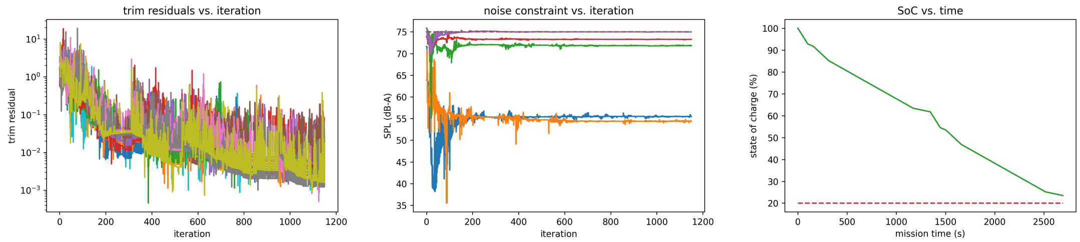

Fig. 13 Trim and noise constraints vs. optimization iteration and optimized state-of-charge vs. mission time

2. Summary of full-scale optimization

We summarize high-level design variables before and after optimization in Tab. 4. We note that for the wing area and the fuselage length (optimized by changing the tail moment arm), the optimizer reached the lower bound set for those variables. This suggests that the vehicle gross weight could potentially be reduced further by relaxing the lower bounds. For the rotor radii, the order from left to right is front-outer, front-inner, rear-outer, and rear-inner. We acknowledge that for practical purposes, it may not be feasible to size the lift rotors differently.

Table 4 Summary of high-level design variable changes

Variable	Initial	Optimized
Wing area (ft^2)	210	160
Wing aspect ratio	13	11.6
Fuselage length (ft)	30	27.0
Battery weight (lb)	1980	1675
Lift rotor radii (ft)	[5, 5, 5, 5]	[4.0, 4.4, 4.2, 4.2]

VII. Conclusion

In this paper, we demonstrate the application of large-scale multidisciplinary design optimization (MDO) to NASA's lift-plus-cruise electric air taxi concept. This is achieved by constructing a comprehensive system model of the aircraft for all its major sub-disciplines, using low-to mid-fidelity physics-based models. We improve the modeling fidelity over our previous studies of the lift-plus-cruise concept by including in-the-loop structural analysis of the wing as well as improved aeroacoustic and rotor-aerodynamic models. In addition, we expand the number of design conditions that are modeled to include several steady (e.g., cruise), quasi-steady (transition), off-design (one-engine-inoperative), and structural sizing scenarios, amounting to a total of 18 design conditions. We solve a gross weight minimization problem with over 300 design variables and over 200 constraints across all discipline models. Solving this problem is made possible through a newly developed aircraft design software library called the Comprehensive Aircraft high-Dimensional Design Environment (CADDEE), which enables the assembly of various sub-discipline models.

Results show a gross weight reduction of about 10% over the initial design with all major constraints (e.g., aircraft trim, noise) being satisfied. The total optimization time is about 17 hours. These results demonstrate the feasibility of applying large-scale MDO to the aircraft conceptual design problem to efficiently explore the design space, using physics-based models in combination with gradient-based optimization. Despite these results, there are several areas for improvement, mostly pertaining to raising the modeling fidelity of the aircraft sub-disciplines. For example, we plan to use the Reissner–Mindlin shell theory to more accurately model the wing structure. In addition, we have implemented but not tested the Brooks–Pope–Marcolini broadband noise model for more accurate aeroacoustic results. Lastly, we would like to further expand the scope of design conditions that we consider to also include fully dynamic cases such as a gust response or wing flutter.

Acknowledgments

The material presented in this paper is supported by NASA under award No. 80NSSC21M0070.

References

[1] Sheehan, V., "Vertical Flight Society Electric VTOL Directory Hits 700 Concepts," , 2022-08-16. Https://vtol.org/news/press-release-vfs-electric-vtol-directory-hits-700-concepts.

[2] Raymer, D., *Aircraft design: a conceptual approach*, American Institute of Aeronautics and Astronautics, Inc., 2012.

[3] Roskam, J., *Airplane Design Parts I through VIII*, 2003.

[4] Torenbeek, E., *Synthesis of subsonic airplane design: an introduction to the preliminary design of subsonic general aviation and transport aircraft, with emphasis on layout, aerodynamic design, propulsion and performance*, Springer Science & Business Media, 2013.

[5] McCullers, L., "Aircraft configuration optimization including optimized flight profiles," *NASA. Langley Research Center Recent Experiences in Multidisciplinary Analysis and Optimization, Part 1*, 1984.

[6] Johnson, W., "NDARC NASA design and analysis of rotorcraft," Tech. rep., 2017.

[7] Nagel, B., Böhnke, D., Gollnick, V., Schmollgruber, P., Rizzi, A., La Rocca, G., and Alonso, J. J., "Communication in aircraft design: Can we establish a common language," *28th International Congress of the Aeronautical Sciences*, Vol. 201, 2012.

[8] Welstead, J. R., Caldwell, D., Condotta, R., and Monroe, N., "An Overview of the Layered and Extensible Aircraft Performance System (LEAPS) Development," *2018 AIAA Aerospace Sciences Meeting*, 2018, p. 1754.

[9] Lukaczyk, T. W., Wendorff, A. D., Colonno, M., Economon, T. D., Alonso, J. J., Orra, T. H., and Ilario, C., "SUAVE: an open-source environment for multi-fidelity conceptual vehicle design," *16th AIAA/ISSMO Multidisciplinary Analysis and Optimization Conference*, 2015, p. 3087.

[10] De Vries, R., Hoogreef, M. F., and Vos, R., "Range equation for hybrid-electric aircraft with constant power split," *Journal of Aircraft*, Vol. 57, No. 3, 2020, pp. 552–557.

[11] Finger, D. F., de Vries, R., Vos, R., Braun, C., and Bil, C., "A comparison of hybrid-electric aircraft sizing methods," *AIAA scitech 2020 forum*, 2020, p. 1006.

[12] Chakraborty, I., and Mishra, A. A., "Generalized Energy-Based Flight Vehicle Sizing and Performance Analysis Methodology," *Journal of Aircraft*, Vol. 58, No. 4, 2021, pp. 762–780.

[13] Finger, D. F., Bil, C., and Braun, C., "Initial sizing methodology for hybrid-electric general aviation aircraft," *Journal of Aircraft*, Vol. 57, No. 2, 2020, pp. 245–255.

[14] Hwang, J., and Martins, J. R., "GeoMACH: geometry-centric MDAO of aircraft configurations with high fidelity," *12th AIAA Aviation Technology, Integration, and Operations (ATIO) Conference and 14th AIAA/ISSMO Multidisciplinary Analysis and Optimization Conference*, 2012, p. 5605.

[15] Hahn, A., "Vehicle sketch pad: a parametric geometry modeler for conceptual aircraft design," *48th AIAA Aerospace Sciences Meeting Including the New Horizons Forum and Aerospace Exposition*, 2010, p. 657.

[16] Chauhan, S. S., and Martins, J. R., "Tilt-wing eVTOL takeoff trajectory optimization," *Journal of Aircraft*, Vol. 57, No. 1, 2020, pp. 93–112.

[17] Orndorff, N. C., and Hwang, J. T., "Investigation of optimal air-taxi transition profiles using direct-transcription trajectory optimization," *AIAA AVIATION 2022 Forum*, 2022, p. 3485.

[18] Orndorff, N. C., Sarojini, D., Scotzniovsky, L., Gill, H., Lee, S., Cheng, Z., Zhao, S., Mi, C., and Hwang, J. T., "Air-taxi transition trajectory optimization with physics-based models," *AIAA SCITECH 2023 Forum*, 2023, p. 0324.

[19] Kaneko, S., and Martins, J. R., "Simultaneous Optimization of Conceptual Design and Takeoff Trajectory of a Lift-Plus-Cruise UAV," *10th Autonomous VTOL Technical Meeting*, 2023.

[20] Riboldi, C. E., Gualdoni, F., and Trainelli, L., "Preliminary weight sizing of light pure-electric and hybrid-electric aircraft," *Transportation Research Procedia*, Vol. 29, 2018, pp. 376–389.

[21] Winter, T. F., Robinson, J., Gamez, A., and Nascenzi, T., "Conceptual Design Structural Sizing for Urban Air Mobility," *AIAA Scitech 2021 Forum*, 2021, p. 1722.

[22] Nascenzi, T., Cuatt, T., Winter, T. F., Ruh, M. L., Sarojini, D., Hwang, J. T., and Kiani, S., "Physics-based Surrogate Models for UAM Weight Prediction," *AIAA SCITECH 2023 Forum*, 2023, p. 1360.

[23] Palaia, G., Zanetti, D., Salem, K. A., Cipolla, V., and Binante, V., "THEA-CODE: a design tool for the conceptual design of hybrid-electric aircraft with conventional or unconventional airframe configurations," *Mechanics & Industry*, Vol. 22, 2021, p. 19.

[24] Palaia, G., Abu Salem, K., Cipolla, V., Binante, V., and Zanetti, D., "A conceptual design methodology for e-VTOL aircraft for urban air mobility," *Applied Sciences*, Vol. 11, No. 22, 2021, p. 10815.

[25] Brown, A., and Harris, W. L., "Vehicle design and optimization model for urban air mobility," *Journal of Aircraft*, Vol. 57, No. 6, 2020, pp. 1003–1013.

[26] Ugwueze, O., Statheros, T., Horri, N., Bromfield, M. A., and Simo, J., "An Efficient and Robust Sizing Method for eVTOL Aircraft Configurations in Conceptual Design," *Aerospace*, Vol. 10, No. 3, 2023, p. 311.

[27] Sarojini, D., Ruh, M. L., Joshy, A. J., Yan, J., Ivanov, A. K., Scotzniovsky, L., Fletcher, A. H., Orndorff, N. C., Sperry, M., Gandarillas, V. E., et al., "Large-Scale Multidisciplinary Design Optimization of an eVTOL Aircraft using Comprehensive Analysis," *AIAA SCITECH 2023 Forum*, 2023, p. 0146.

[28] Ruh, M. L., Sarojini, D., Fletcher, A., Asher, I., and Hwang, J. T., "Large-scale multidisciplinary design optimization of the NASA lift-plus-cruise concept using a novel aircraft design framework," *arXiv preprint arXiv:2304.14889*, 2023.

[29] Hwang, J. T., and Ning, A., "Large-scale multidisciplinary optimization of an electric aircraft for on-demand mobility," *2018 AIAA/ASCE/AHS/ASC Structures, Structural Dynamics, and Materials Conference*, 2018, p. 1384.

[30] Ha, T. H., Lee, K., and Hwang, J. T., "Large-scale multidisciplinary optimization under uncertainty for electric vertical takeoff and landing aircraft," *AIAA Scitech 2020 Forum*, 2020, p. 0904.

[31] Orndorff, N. C., Wang, B., Ruh, M. L., Fletcher, A. H., and Hwang, J., "Gradient-based sizing optimization of power-beaming-enabled aircraft," *AIAA Aviation 2023 Forum*, 2023.

[32] Warner, M. A. P., Fletcher, A. H., van Schie, S. P. C., and Hwang, J. T., "A Method for Modular MDO Model Assembly via a Solver Independent Field Representation," *AIAA SciTech 2024 Forum*, 2024. In review.

[33] Gandarillas, V., Joshy, A. J., Sperry, M. Z., Ivanov, A. K., and Hwang, J. T., "A graph-based methodology for constructing computational models that automates adjoint-based sensitivity analysis," *Structural and Multidisciplinary Optimization*, 2022.

[34] Anderson Jr, J. D., *Fundamentals of aerodynamics*, Tata McGraw-Hill Education, 2010.

[35] Katz, J., and Plotkin, A., *Low-speed aerodynamics*, Vol. 13, Cambridge university press, 2001.

[36] Johnson, W., *Noise*, Cambridge Aerospace Series, Cambridge University Press, 2013, p. 493–544. https://doi.org/10.1017/CBO9781139235655.015.

[37] Burton, T., Jenkins, N., Sharpe, D., and Bossanyi, E., *Wind energy handbook*, John Wiley & Sons, 2011.

[38] Glauert, H., "Airplane propellers," *Aerodynamic theory*, Springer, 1935, pp. 169–360.

[39] Mahmuddin, F., "Rotor blade performance analysis with blade element momentum theory," *Energy Procedia*, Vol. 105, 2017, pp. 1123–1129.

[40] Madsen, H. A., Bak, C., Døssing, M., Mikkelsen, R., and Øye, S., "Validation and modification of the blade element momentum theory based on comparisons with actuator disc simulations," *Wind Energy: An International Journal for Progress and Applications in Wind Power Conversion Technology*, Vol. 13, No. 4, 2010, pp. 373–389. https://doi.org/10.1002/we.359.

[41] Ingram, G., "Wind turbine blade analysis using the blade element momentum method. version 1.1," *Durham University, Durham*, , No. 2011, 2011.

[42] Ning, S. A., "A simple solution method for the blade element momentum equations with guaranteed convergence," *Wind Energy*, Vol. 17, No. 9, 2014, pp. 1327–1345.

[43] Ruh, M. L., and Hwang, J. T., "Robust modeling and optimal design of rotors using blade element momentum theory," *AIAA AVIATION 2021 FORUM*, 2021, p. 2598.

[44] Pitt, D. M., and Peters, D. A., "Theoretical prediction of dynamic-inflow derivatives," 1980.

[45] Johnson, W., *Rotorcraft aeromechanics*, Vol. 36, Cambridge University Press, 2013.

[46] Orndorff, N. C., Wang, B., Ruh, M. L., Fletcher, A., and Hwang, J. T., "Gradient-based sizing optimization of power-beaming-enabled aircraft," *AIAA AVIATION 2023 Forum*, 2023, p. 4019.

[47] Logan, D. L., *First Course in the Finite Element Method, Enhanced Edition, SI Version*, Cengage Learning, 2022.

[48] Chauhan, S. S., and Martins, J. R., "Low-fidelity aerostructural optimization of aircraft wings with a simplified wingbox model using OpenAeroStruct," *EngOpt 2018 Proceedings of the 6th International Conference on Engineering Optimization*, Springer, 2019, pp. 418–431. https://doi.org/10.1007/978-3-319-97773-7_38.

[49] Sarojini, D., "Structural analysis and optimization of aircraft wings through dimensional reduction," Ph.D. thesis, Georgia Institute of Technology, 2021.

[50] Young, W. C., Budynas, R. G., and Sadegh, A. M., *Roark's formulas for stress and strain*, McGraw-Hill Education, 2012.

[51] Cesnik, C. E., and Hodges, D. H., "VABS: a new concept for composite rotor blade cross-sectional modeling," *Journal of the American helicopter society*, Vol. 42, No. 1, 1997, pp. 27–38.

[52] Xie, J., Sarojini, D., Cai, Y., Corman, J. A., and Mavris, D. N., "Certification-Driven Platform for Multidisciplinary Design Space Exploration in Airframe Preliminary Design," *Journal of Aircraft*, Vol. 59, No. 2, 2022, pp. 329–349. https://doi.org/10.2514/1.C036328.

[53] Xie, J., Cai, Y., Sarojini, D., Harrison, E., and Mavris, D. N., "Vertical Tail Sizing and Power Split Optimization for the PEGASUS Concept Considering Certification Requirements," *AIAA AVIATION 2022 Forum*, 2022, p. 3204. https://doi.org/https://doi.org/10.2514/6.2022-3204.

[54] Moorhouse, D., and Woodcock, R., *US Military Specification Mil-F-8785C*, US Department of Defense, 1980.

[55] ADS-33E-PRF, A. D. S., *Handling Qualities Requirements for Military Rotorcraft*, 2000.

[56] Sarojini, D., Ruh, M. L., Sperry, M., Yan, J., Fletcher, A., Joshy, A. J., Scotzniovsky, L., Ivanov, A., Orndorff, N., Gandarillas, V., Asher, I., Chambers, J., Gill, H., Lee, S., Cheng, Z., Rodriguez, G., Zhao, S., Mi, C., Nascenzi, T., Cuatt, T., Winter, T., Guibert, A., Cronk, A., Kim, A., Meng, S., and Hwang, J. T., "Large-Scale Multidisciplinary Design Optimization of an eVTOL Aircraft Using Comprehensive Analysis," *AIAA SciTech Forum*, AIAA Paper 2023–0146, Jan. 2023. https://doi.org/10.2514/6.2023-0146.

[57] Orndorff, N., Scotzniovsky, L., Sarojini, D., Gill, H., Lee, S., Cheng, Z., Zhao, S., Mi, C., and Hwang, J. T., "Air-Taxi Transition Trajectory Optimization with Physics-Based Models," *AIAA SciTech Forum*, AIAA Paper 2022–3485, Jan. 2023. https://doi.org/10.2514/6.2022-3485.

[58] Barry, F. W., and Magliozzi, B., "Noise Detectability Prediction Method for Low Tip Speed Propellers," Tech. Rep. AFAPL–TR–71–37, Air Force Aero Propulsion Laboratory, June 1971.

[59] Schlegel, R., King, R., and Mull, H., "Helicopter Rotor Noise Generation and Propagation," Tech. Rep. USAAVLABS–TR–66–4, U.S. Army Aviation Materiel Laboratories, October 1966.

[60] Lowson, M. V., and Ollerhead, J. B., "A Theoretical Study of Helicopter Rotor Noise," *Journal of Sound Vibration*, Vol. 9, No. 2, 1969, pp. 197–222. https://doi.org/10.1016/0022-460X(69)90028-5.

[61] Gill, H., and Lee, S., "Development of a New Empirical Rotor Broadband Noise Prediction Models for Urban Air Mobility Applications," *Proceedings of the Science and Technology Forum and Exposition*, AIAA, Jan. 2024.

[62] Gill, H., Lee, S., Ruh, M., and Hwang, J. T., "Applicability of Low-Fidelity Tonal and Broadband Noise Models on Small-Scale Rotors," *AIAA Sci Tech Forum*, AIAA Paper 2023–1547, Jan. 2023. https://doi.org/10.2514/6.2023-1547.

[63] Guttin, L., "On the Sound Field of a rotating Propeller," Tech. Rep. NACA–TM–1195, National Advisory Committee for Aeronautics, 1936.

[64] Sears, W. R., and Sparks, B. O., "On the Reaction of an Elastic Wing to Vertical Gusts," *Journal of the Aeronautical Sciences*, Vol. 9, No. 2, 1941, pp. 64–81. https://doi.org/10.2514/8.10802.

[65] Kvurt, A., and Stalnov, O., "From the Blade Geometry to Prediction of Tonal Noise Component in Hover," *AIAA/CEAS Aeroacoustics Conference*, AIAA Paper 2022–3076, June 2022. https://doi.org/10.2514/6.2022-3076.

[66] Whelchel, J., Alexander, W. N., and Intaratep, N., "Propeller Noise in Confined Anechoic and Open Environments," *AIAA SciTech Forum*, AIAA Paper 2020–1252, Jan. 2020. https://doi.org/10.2514/6.2020-1252.

[67] Tinney, C., and Valdez, J., "Acoustic Scaling for Small Rotors in Hover," AHS International 75^{th} Annual Forum and Technology Display, Philadelphia, Pennsylvania, May 14–15, 2019.

[68] Zawodny, N. S., Pettingill, N. A., Lopes, L. V., and Ingraham, D., "Experimental Validation of an Acoustically and Aerodynamically Optimized UAM Proprotor Part 1: Test Setup and Results," Tech. Rep. NASA–TM–20220015637, National Aeronautics and Space Administration, February 2023.

[69] Weatheritt, J., and Sandberg, R., "A Novel Evolutionary Algorithm Applied to Algebraic Modifications of the RANS Stress-Strain Relationship," *Journal of Computational Physics*, Vol. 325, 2016, pp. 22–37. https://doi.org/10.1016/j.jcp.2016.08.015.

[70] Fritsch, D. J., Vishwanathan, V., Roy, C. J., Lowe, K. T., Devenport, W. J., Croaker, P., Tkachenko, O., Pook, D., Lane, G., Shubham, S., and Sandberg, R. D., "Modeling the Surface Pressure Spectrum Beneath Turbulent Boundary Layers in Pressure Gradients," *AIAA Journal*, Vol. 61, No. 5, 2023, pp. 1–20. https://doi.org/10.2514/1.J062074.

[71] Lee, S., "Empirical Wall-Pressure Spectral Modeling for Zero and Adverse Pressure Gradient Flows," *AIAA Journal*, Vol. 56, No. 5, 2018, pp. 1818–1829. https://doi.org/10.2514/1.J056528.

[72] Lee, S., Ayton, L., Bertagnolio, F., Moreau, S., Chong, T. P., and Joseph, P., "Turbulent Boundary Layer Trailing-Edge Noise: Theory, Computation, Experiment, and Application," *Progress in Aerospace Sciences*, Vol. 126, Oct. 2021, p. 100737. https://doi.org/10.1016/j.paerosci.2021.100737.

[73] Li, S., and Lee, S., "Prediction of Rotorcraft Broadband Trailing-Edge Noise and Parameter Sensitivity Study," *Journal of the American Helicopter Society*, Vol. 65, No. 4, 2020, pp. 1–14. https://doi.org/10.4050/JAHS.65.042006.

[74] Sarojini, D., Wolf, L., Doring, R., Despins, R., Lee, A., Salkoff, E., Kim, K., Ruh, M. L., Yan, J., Orndorff, N., Scotzniovsky, L., Joseph, C., Anderson, R. M., Ning, A., Gill, H., Lee, S., Cheng, Z., Mi, C., Cronk, A., Guibert, A., Kim, A., Meng, S., Silva, C., and Hwang, J. T., "Review of Computational Models for Large-Scale MDAO of Urban Air Mobility Concepts," *Proceedings of the Science and Technology Forum and Exposition*, AIAA, Jan. 2024.

[75] Vegh, J. M., Botero, E., Clark, M., Smart, J., and Alonso, J. J., "Current Capabilities and Challenges of NDARC and SUAVE for eVTOL Aircraft Design and Analysis," *2019 AIAA/IEEE Electric Aircraft Technologies Symposium (EATS)*, 2019, pp. 1–19. https://doi.org/10.2514/6.2019-4505.

[76] Brown, A., and Harris, W. L., "Vehicle Design and Optimization Model for Urban Air Mobility," *Journal of Aircraft*, Vol. 57, No. 6, 2020. https://doi.org/10.2514/1.C035756.

[77] Afonso, F., Ferreira, A., Ribeiro, I., Lau, F., and Suleman, A., "On the design of environmentally sustainable aircraft for urban air mobility," *Transportation Research Part D: Transport and Environment*, Vol. 91, 2021, p. 102688. https://doi.org/https://doi.org/10.1016/j.trd.2020.102688.

[78] Htwe, N. H. H., "Design of 50 kw Permanent Magnet Synchronous Motor for HEV," *Iconic Research and Engineering Journals*, Vol. 3, No. 2, 2019.

[79] Mi, C., Filippa, M., Liu, W., and Ma, R., "Analytical Method for Predicting the Air-Gap Flux of Interior-Type Permanent-Magnet Machines," *IEEE Transactions on Magnetics*, Vol. 40, No. 1, 2004. https://doi.org/10.1109/TMAG.2003.821562.

[80] Lu, D., and Kar, N. C., "A review of flux-weakening control in permanent magnet synchronous machines," *2010 IEEE Vehicle Power and Propulsion Conference*, 2010, pp. 1–6. https://doi.org/10.1109/VPPC.2010.5728986.

[81] Zhao, S. F., Huang, X. Y., Fang, Y. T., and Li, J., "A control scheme for a High Speed Railway traction system based on high power PMSM," *2015 6th International Conference on Power Electronics Systems and Applications (PESA)*, 2015, pp. 1–8. https://doi.org/10.1109/PESA.2015.7398905.

[82] Sperry, M. Z., Kondap, K., and Hwang, J. T., "Static Task Scheduling for Parallel Execution of Large-Scale Multidisciplinary Design Optimization Models," *AIAA SCITECH 2024 Forum*, 2024.

[83] Gabriel, E., Fagg, G. E., Bosilca, G., Angskun, T., Dongarra, J. J., Squyres, J. M., Sahay, V., Kambadur, P., Barrett, B., Lumsdaine, A., et al., "Open MPI: Goals, concept, and design of a next generation MPI implementation," *Recent Advances in Parallel Virtual Machine and Message Passing Interface: 11th European PVM/MPI Users' Group Meeting Budapest, Hungary, September 19-22, 2004. Proceedings 11*, Springer, 2004, pp. 97–104.

[84] Kwok, Y.-K., and Ahmad, I., "Static Scheduling Algorithms for Allocating Directed Task Graphs to Multiprocessors," *ACM Comput. Surv.*, Vol. 31, No. 4, 1999, p. 406–471. https://doi.org/10.1145/344588.344618, URL https://doi.org/10.1145/344588.344618.

[85] Gill, P. E., Murray, W., and Saunders, M. A., "SNOPT: An SQP algorithm for large-scale constrained optimization," *SIAM review*, Vol. 47, No. 1, 2005, pp. 99–131.

[86] Silva, C., Johnson, W. R., Solis, E., Patterson, M. D., and Antcliff, K. R., "VTOL urban air mobility concept vehicles for technology development," *2018 Aviation Technology, Integration, and Operations Conference*, 2018, p. 3847. https://doi.org/10.2514/6.2018-3847.